Biochimica et Biophysica Acta 1818 (2012) 367–374

Contents lists available at SciVerse ScienceDirect

Biochimica et Biophysica Acta

journal homepage: www.elsevier.com/locate/bbamem

Voltage-dependent inactivation of the plasmodial surface anion channel via a cleavable cytoplasmic component

Abdulnaser Alkhalil [1], Liang Hong, Wang Nguitragool, Sanjay A. Desai *

The Laboratory of Malaria and Vector Research, National Institute of Allergy and Infectious Diseases, National Institutes of Health, Rockville, MD 20852, USA

ARTICLE INFO

Article history:
Received 12 July 2011
Received in revised form 17 October 2011
Accepted 8 November 2011
Available online 13 November 2011

Keywords:
PSAC
Voltage-dependent inactivation
Patch-clamp
Malaria
Antimalarial drug targets
Clag genes

ABSTRACT

Erythrocytes infected with malaria parasites have increased permeability to ions and various nutrient solutes, mediated by a parasite ion channel known as the plasmodial surface anion channel (PSAC). The parasite *clag3* gene family encodes PSAC activity, but there may also be additional unidentified components of this channel. Consistent with a lack of *clag3* homology to genes of other ion channels, PSAC has a number of unusual functional properties. Here, we report that PSAC exhibits an unusual form of voltage-dependent inactivation. Inactivation was readily detected in the whole-cell patch-clamp configuration after steps to negative membrane potentials. The fraction of current that inactivates, its kinetics, and the rate of recovery were all voltage-dependent, though with a modest effective valence (0.7 ± 0.1 elementary charges). These properties were not affected by solution composition or charge carrier, suggesting inactivation intrinsic to the channel protein. Intriguingly, inactivation was absent in cell-attached recordings and took several minutes to appear after obtaining the whole-cell configuration, suggesting interactions with soluble cytosolic components. Inactivation could also be largely abolished by application of intracellular, but not extracellular protease. The findings implicate inactivation via a charged cytoplasmic channel domain. This domain may be tethered to one or more soluble intracellular components under physiological conditions.

Published by Elsevier B.V.

1. Introduction

Malaria parasite-infected erythrocytes have increased permeability to diverse solutes including anions, amino acids, sugars, purines, and vitamins, and organic cations [1–6]. Although host transporters may contribute to the uptake of some solutes, a parasite-derived ion channel known as the plasmodial surface anion channel (PSAC) appears to be the primary uptake mechanism for most solutes [7]. Recently, genetic mapping and DNA transfection experiments in the human pathogen *Plasmodium falciparum* have implicated two paralogous *clag3* genes in formation of PSAC [8]. The *clag3* products do not resemble known ion channel proteins and were previously assumed to function in cytoadherence or host cell invasion [9,10]. Because both PSAC activity and *clag* genes are conserved in divergent malaria parasites [11,12], increased permeability of infected cells is presumed to serve an important role, possibly in nutrient acquisition by the intracellular parasite. High-throughput screening has identified potent and specific PSAC inhibitors that may be starting points for future antimalarial drugs [13].

In addition to its potential as a therapeutic target, PSAC exhibits a number of unusual functional properties. Intriguingly, although the channel is broadly permeant to bulky organic solutes that carry either net positive or negative charge, it excludes the small Na^+ ion; Na^+ exclusion is required to prevent osmotic lysis of infected cells in the host bloodstream [14]. Other unusual properties of PSAC include unexpected interactions between permeating solutes and inhibitors [15], atypical voltage-dependent gating [16], and a surprisingly small single channel conductance for a broad permeability channel, only ~20 pS in 1.1 M Cl^-.

Here, we report an unusual form of voltage-dependent inactivation in PSAC. Inactivation, a reversible decrease in ion flux through channels despite a sustained driving force, has been well-characterized in Na^+, K^+, and Ca^{++} channels and is less recognized among anion channels. A previous study observed voltage-dependent changes in infected cell currents and proposed that they may account for discrepancies in the patch-clamp findings of various groups [17]. Because neither the biophysical properties nor the mechanism of inactivation was explored there, it is not clear whether their recordings reflect voltage-dependent inactivation of PSAC, as described here.

Although it has a modest voltage dependence, PSAC inactivation has a number of unique features that provide insights into the permeation process. Our studies implicate a cytoplasmic component of the

Abbreviations: PSAC, plasmodial surface anion channel; clag, cytoadherence linked antigen; V_m, membrane potential; z_g, effective valence of inactivating particle; HEPES, 4-(2-hydroxyethyl)-1-piperazineethanesulfonic acid

* Corresponding author at: Room 3W-01, 12735 Twinbrook Parkway, NIAID/NIH, Rockville, MD, 20852. USA. Tel.: +1 301 4357552; fax: +1 301 402 2201.
E-mail address: sdesai@niaid.nih.gov (S.A. Desai).
[1] Present address: Virology Division, US Army Medical Research Institute of Infectious Diseases, 1425 Porter Street, Fort Detrick, MD 21702, USA.

0005-2736/$ – see front matter. Published by Elsevier B.V.
doi:10.1016/j.bbamem.2011.11.010

channel in PSAC inactivation; we describe charged domains on the *clag3* product that may be involved.

2. Materials and methods

2.1. Parasite culture

P. falciparum malaria parasites were cultivated in O^+ human red blood cells using standard methods. Infected erythrocytes were harvested and used for experiments at the trophozoite stage. Four divergent parasite lines (Indo 1, HB3, 3D7A, and 7G8) produced similar results, which were pooled in this study.

2.2. Electrophysiology

Single channel and whole-cell patch-clamp recordings of infected RBCs were obtained as previously described [18]. Unless otherwise indicated, these experiments utilized symmetrical bath and pipette solutions of (in mM): 1000 choline-Cl, 115 NaCl, 10 $MgCl_2$, 5 $CaCl_2$, 20 Na-HEPES, pH 7.4 (solution A). Pipettes were pulled from quartz glass to tip diameters<0.5 μm, coated with Sylgard 184 elastomer (Dow Corning), and had resistances of 1–4 MΩ in solution A. Seal resistances were ≥100 GΩ. Recordings were obtained in Clampex 9.0 (Axon Instruments), filtered at 5 kHz with an 8 pole Bessel filter, and digitized at 100 kHz.

The whole-cell configuration was typically obtained by electroporation of the patch with brief voltage pulses (500–900 mV, ≤1 ms duration). Where attempted, patch excision from the cell-attached configuration was performed by moving the clamped cell through the air-solution interface; although this procedure invariably dislodged the cell, we could not exclude formation of a membrane-bound vesicle with retained cytosol at the pipette tip.

Experiments using pronase E from *S. griseus* (CAS Number 9036-06-0, Sigma-Aldrich) were carried out in solution A; control experiments confirmed that protease activity is preserved in this hypertonic solution (not shown). Fresh solutions containing pronase E were prepared for each experiment; similar effects on PSAC activity were observed using protease concentrations between 25 and 100 μg/mL. For intracellular application, the pipette tip was first filled with protease-free solution by applying negative pressure to the patch pipette. The pipette was then backfilled with solution A containing pronase E at indicated concentrations. This two-step procedure permitted durable seals on infected cells. Diffusion of the protease into the cell after obtaining the whole-cell configuration was typically completed with 10–15 min, based on the kinetics of protease effect on PSAC inactivation.

Extracellular application of pronase E was performed in a homemade chamber designed to permit complete solution change around a clamped erythrocyte without adversely affecting seal resistance [19]. In contrast to the more dramatic effects of chymotrypsin [20], extracellular pronase E had a relatively modest effect on transport rates.

2.3. Analyses

Data analysis was performed with in house programs. Curve fitting was done using least squares fitting in SigmaPlot 10.0 (Systat). The fractional current remaining after inactivation at different voltages was fitted to the Boltzmann equation:

$$I_{ss}/I_{peak} = 1/[1 + \exp(w - z_g * V_m)/25.5)], \quad (1)$$

where I_{ss} and I_{peak} are the steady-state inactivated and fully activated currents, respectively. w represents change in free energy associated with the inactivation process at zero membrane potential (V_m). z_g is the effective valence of the inactivating particle and is based on gating charge movement through the entire membrane electric field. The value 25.5 is the product of universal physical constants, kT/q_e at room temperature.

Statistical data are expressed as means ± S.E.M., with n indicating the number of samples. Where comparisons were made, differences between the means of two groups were evaluated using Student's unpaired t tests.

Computational analyses on the CLAG3 protein were performed using net charge values for each residue at physiological pH as in EMBOSS 6.3.1:protein charge (http://emboss.open-bio.org/wiki/Appdoc:Charge). Average local charge was calculated from a moving window of 150 residues centered at each residue along the protein encoded by the PFC0120w gene (*clag3.1*) of the 3D7 parasite line. Window size was adjusted accordingly at the ends of the protein.

3. Results

3.1. PSAC exhibits voltage-dependent inactivation

Whole-cell patch-clamp of uninfected human erythrocytes reveals small conductances difficult to separate from leak through attainable seal resistances [7]. When these studies are carried out with *P. falciparum*-infected erythrocytes, these conductances are significantly greater and exhibit inward rectification (Fig. 1A). Although altered host channels may contribute to the increased currents, PSAC activity is responsible for most of the increase [8,18].

After several minutes of recordings from the cell clamped in Fig. 1A, we applied a modified protocol consisting of 500 ms pulses over the same voltage range. Although the initial response to each voltage pulse was well-preserved, we observed that the currents at large negative membrane potentials (V_m) gradually decreased. These decreases were not seen at positive V_m values and did not depend on the order in which voltage pulses were applied (Fig. 1B–D). Thus, this decay in currents upon application of negative V_m reflects voltage-dependent inactivation, as described for various cation channels. We recognize that complex schema having multiple inactivated states may produce apparent voltage dependence by linking inactivation to the intrinsic voltage dependence of PSAC gating. We also examined the much smaller currents on uninfected RBCs and found that they do not inactivate (Fig. 1E).

3.2. Inactivation is intrinsic to the channel protein

Voltage-dependent inactivation may result from pore block by charged solutes dissolved in the bathing solution [21–25] or may be intrinsic to the channel protein [26–29]. To examine these possible mechanisms in PSAC inactivation, we obtained whole-cell recordings with various solution compositions in both intracellular and extracellular compartments. Because permeating solutes often produce inactivation, we examined PSAC currents with Br^- as the principal charge carrier and found inactivation occurred with comparable kinetics and degree (Fig. 2). Other experiments confirmed that removal of Ca^{++}, Mg^{++}, HEPES from both pipette and bath compartments or that changes in Na^+ concentration between 115 and 1145 mM also did not abolish inactivation or alter its properties significantly (not shown). These findings along with effects of protease treatment described below are strong evidence against pore block by dissolved solutes as the basis of PSAC inactivation.

3.3. Steady-state currents are adequately fit by the Boltzmann equation with a small gating charge

Voltage-dependent inactivation yielded steady-state currents that were invariably non-zero despite application of negative V_m values as large as −150 mV. We quantified initial and steady state currents and examined the voltage dependence of their ratio (Fig. 3A). These data

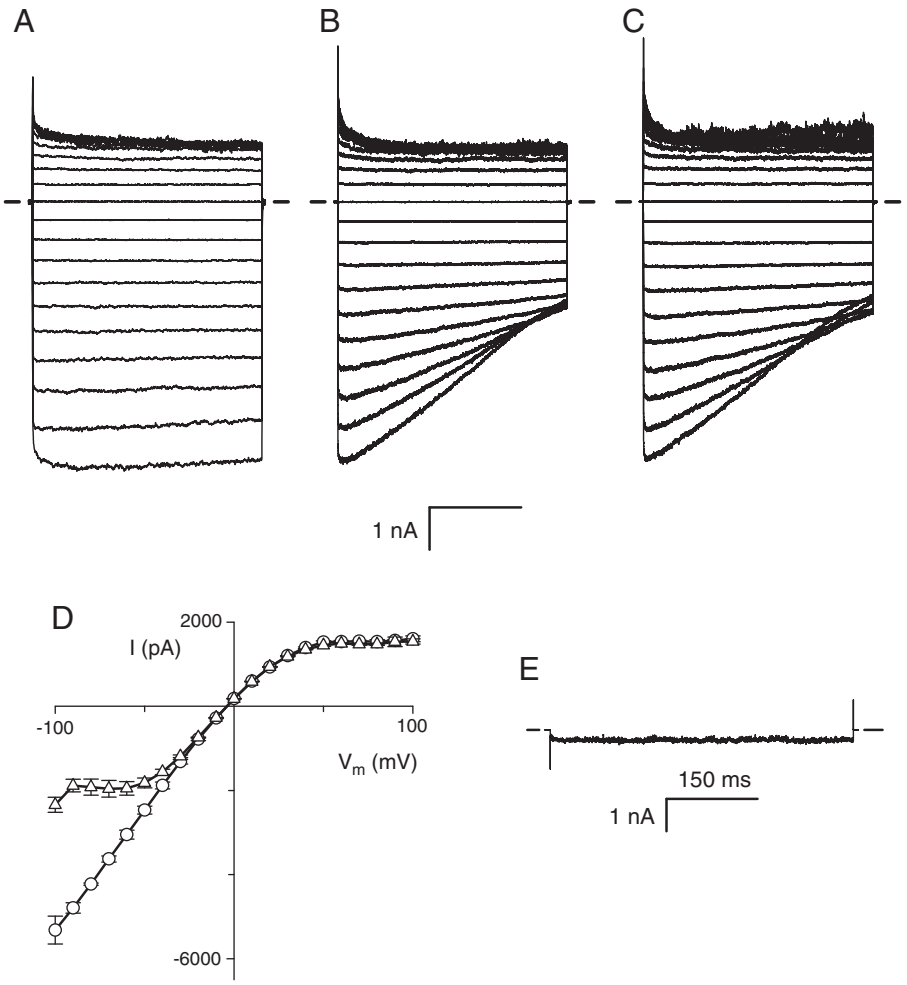

Fig. 1. Voltage-dependent inactivation of currents on infected RBCs, but not on uninfected RBCs. (A–B) Whole-cell currents from an infected RBC in response to voltage pulses between −100 mV and +100 mV in 10 mV increments. Pulses were either 50 ms (A) or 500 ms (B) in duration. In (B), a delay of 10 s between sequential voltage pulses was incorporated to allow complete recovery from inactivation during preceding pulses. While PSAC's intrinsic voltage dependence is apparent in both panels as significantly greater currents at negative V_m, inactivation can only detected with sustained negative V_m. (C) Whole-cell currents from the same cell as panel B, using a protocol with reversed order of voltage pulses. Notice the gradually decreasing currents at negative V_m in panels B and C. Vertical scale bar represents 1 nA for panels A–C; horizontal bar represents 20 ms (A) or 200 ms (B and C). (D) Current–voltage relationships for the cell in panels A–C. Symbols represent the mean currents over a 15 ms period after initiating the voltage pulse or upon steady-state inactivation (circles and triangles, respectively). Error bars represent the S.E.M. of 3–5 consecutive trials. (E) Current response on an uninfected RBC to a 500 ms voltage pulse of −100 mV.

were fitted to the Boltzmann equation (Eq. (1); solid curve, Fig. 3B), which assumes a single population of channels with uniform susceptibility to inactivation and predicts macroscopic steady-state currents as a function of the imposed V_m. The inactivating particle's effective valence, z_g, was 0.62 ± 0.09 (range of 0.59–0.93 for 5 other cells, not shown), revealing relatively weak voltage dependence of inactivation for this channel. This effective valence assumes a net change that moves through the full extent of the membrane electric field; if the responsible charges only move through a fraction of the membrane's electric field, as appears likely, a greater net charge would be required to produce the observed voltage dependence [30].

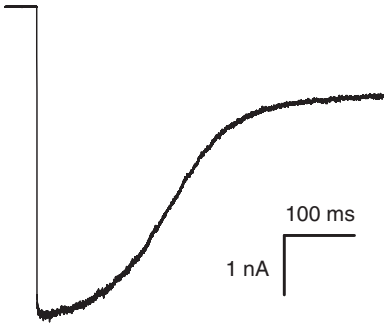

Fig. 2. Degree and kinetics of inactivation are not influenced by solution composition. Whole current in response to a 500 ms voltage step to −100 mV with 500 mM NaBr, 5 mM $CaCl_2$, 10 mM $MgCl_2$, 20 mM Na-HEPES, pH 7.5 in both bath and pipette. $n = 2$ cells.

The kinetics of inactivation was also voltage-dependent because the halftime of inactivation increased in a monotonic fashion with depolarizing V_m pulses (Fig. 3C). These biophysical properties suggest inactivation results from relatively slow rearrangements in the channel protein that are facilitated by negative V_m.

3.4. Recovery from inactivation has slow kinetics and is voltage-dependent

As expected for voltage-induced deformations of a channel protein, inactivation was found to be a fully reversible process with recovery kinetics dependent on the applied V_m. The kinetics at zero V_m was examined with the voltage pulse protocol described in Fig. 4A. This infected cell's currents decayed from −6.0 to −2.4 nA over 500 ms under a constant V_m of −100 mV to approach an inactivated steady-state. Repeated applications of this initial hyperpolarizing voltage step produced reproducible currents and

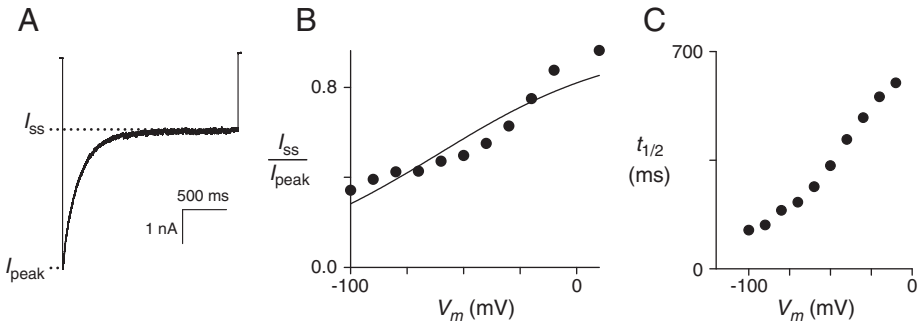

Fig. 3. Steady-state level of inactivation and kinetics are consistent with movement of charged residues. (A) Whole-cell recording in response to a 2 s pulse to a V_m of −100 mV with solution A in both bath and pipette. The non-zero steady-state inactivated current (I_{ss}) is less than the peak initial current (I_{peak}). (B) The ratio of I_{ss} to I_{peak} as a function of imposed V_m for the cell in panel (A). The solid line represents a least squares best fit to Eq. (1) with parameter estimates of $z_g = 0.62 \pm 0.09$ charge equivalents and $w = -38 \pm 6$ mV. (C) Halftime of inactivation process, defined as time to reaching $(I_{ss} + I_{peak})/2$, as a function of V_m for the same cell. Notice that $t_{½}$ increases as V_m is raised.

inactivation kinetics, as indicated by the superposition of traces in the ensemble. After this hyperpolarizing pulse, a variable duration step to V_m of 0 mV was applied to allow increasing degrees of recovery from inactivation. A subsequent test pulse to -100 mV was then used to expose the extent of recovery. The currents in response to this test pulse increased as the duration of the preceding step to 0 mV was increased. Because these currents reached plateau levels that matched the current at the start of the first pulse when the intervening step to 0 mV was ≥1500 ms in duration, the full time course of recovery from inactivation could be followed with these test pulses. Recovery

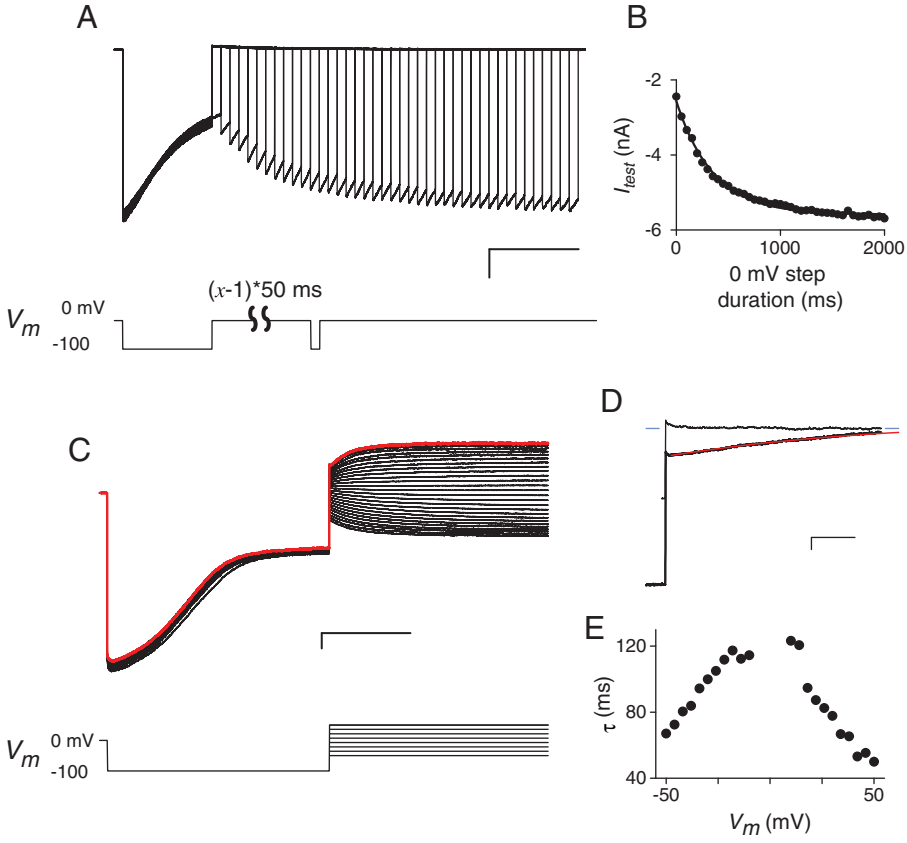

Fig. 4. Kinetics of recovery from inactivation. (A) Ensemble of 41 consecutive traces recorded from a cell in the whole-cell configuration. After a 500 ms voltage pulse to V_m of −100 mV to produce near complete inactivation, a voltage step to 0 mV was applied for a variable duration (0 to 2000 ms in 50 ms increments) to allow differing amounts of recovery from inactivation. Recovery was then quantified by measuring the response to a 50 ms test pulse to −100 mV. The sweep-to-sweep start time was set at 7 s to allow full recovery from inactivation after each trace. Scale bars represent 1 nA/500 ms. The voltage pulse protocol is shown below the traces. Note the gradually increasing currents in response to the test pulse with increasing duration of the preceding step to 0 mV. (B) The mean current in response to the test pulses in (A) vs. the duration of the step to 0 mV. The solid line represents the best fit to $y = y_o + a^*\exp(-x/b)$ with a time constant, b, of 354 ± 11 ms. (C) Ensemble of 26 consecutive traces recorded using the voltage pulse protocol shown below the traces. The protocol consists of a 500 ms prepulse to −100 mV to produce inactivation followed by a 500 ms step to voltages between −50 and +50 mV in 4 mV increments. The last trace is shown in red. Sweep-to-sweep start time was 7 s. Scale bars, 1 nA/200 ms. (D) Expanded view of the step to +50 mV from panel (C), showing the kinetics of recovery from inactivation (lower black trace). The upper black trace is the same cell's response to a voltage step to +50 mV from 0 mV holding potential and is a no inactivation control. Because the control trace reaches the steady-state current almost immediately after the voltage step, the gradual increase in current for the lower trace reflects recovery from inactivation. Red line is the best fit to $y = y_o + a^*\exp(-x/\tau_r)$. Blue dashes on both sides of the traces reflect the mean steady-state current for the control trace. Scale bars, 500 pA/10 ms. (E) Voltage dependence of the recovery time constant, τ_r, for the cell in panel (C), determined at each V_m as in panel (D). A similar biphasic dependence was present in recordings from another cell.

followed single exponential kinetics with a time constant of 350 ms (Fig. 4B).

We also examined recovery from inactivation with a separate pulse protocol that applies a variable voltage step after channels have inactivated (Fig. 4C). At each applied voltage, recovery from inactivation was apparent as a gradual increase in current with a steady-state response matching the currents recorded without inactivation (Fig. 4D). The time course of this increase at each voltage was adequately fitted by single exponential kinetics (dashed red trace, Fig. 4D). Interestingly, recovery kinetics exhibited a complex voltage-dependence with the slowest recovery around V_m of 0 mV and faster kinetics with increasing positive or negative V_m (Fig. 4E). This biphasic response is unexpected for simple models of voltage-dependent inactivation, which instead predict a monotonic decrease in recovery time constant with more positive V_m.

3.5. Delayed onset of inactivation after achieving the whole-cell configuration

Although all infected cells with durable whole-cell seals exhibited voltage-dependent inactivation and recovery, these properties were typically not apparent in recordings taken immediately after achieving the whole-cell configuration (Fig. 5A, trace 1). Instead, recordings acquired during the first several minutes revealed PSAC's intrinsic inward-rectifying voltage dependence without current relaxations characteristic of inactivation. Consecutive current traces in response to pulses of identical voltage and duration revealed gradual onset of inactivation. Once this initiation process was completed (e.g. traces 8 and 9 in Fig. 5A), the magnitude and kinetics of inactivation did not change further for the remainder of the whole-cell recording on this and other infected cells, which often lasted up to ~2 h.

We considered two explanations for the delayed onset. One possibility is that the erythrocyte cytosol contains a soluble component that suppresses PSAC inactivation. The washout of this component, which occurs as a byproduct of patch rupture to obtain the whole-cell configuration, may produce inactivation with gradual onset kinetics. In this scenario, the delayed onset presumably reflects slow diffusion of the soluble component through the pipette tip and into the pipette solution. A second explanation for the delayed onset of inactivation is that repeated applications of nonzero membrane potentials after obtaining the whole-cell configuration may alter channel conformation and produce inactivation; this is commonly referred to as “use-dependent inactivation” and has been reported in some channels [31]. To distinguish between these possibilities, we examined development of inactivation without exposing cells to repetitive voltage pulses. We obtained the whole-cell configuration and clamped the membrane at zero V_m, a value near the erythrocyte's physiological V_m of −10 mV. This rest period was maintained for >10 min before a single voltage pulse to -100 mV was applied. This protocol revealed inactivation with unchanged properties (Fig. 5B), excluding use-dependence and favoring derepression of PSAC inactivation upon washout of an unidentified soluble modulator.

3.6. Cell-attached recordings do not reveal inactivation

In contrast to the whole-cell configuration, the cell-attached patch-clamp configuration is not expected to produce washout of cytosolic components. We therefore obtained and analyzed single PSAC recordings in the cell-attached configuration. We then repeatedly applied negative V_m pulses for extended periods to explore possible slow inactivation kinetics. Visual examination of these single channel traces did not reveal voltage-dependent inactivation (Fig. 6, upper trace), but detection may be complicated by PSAC's complex and fast-flickering gating [16]. We therefore averaged consecutive traces from this channel molecule and found no reduction in mean current over the pulse duration (Fig. 6, lower trace), indicating that inactivation does not occur in the cell-attached configuration. This finding is consistent with delayed onset of inactivation after achieving the whole-cell configuration (Fig. 5) and supports a requirement for washout of the erythrocyte cytosol in susceptibility to inactivation.

Mechanical excision of patches [32] may allow detection of PSAC inactivation in single-channel recordings. Unfortunately, we were unable to reproducibly obtain excised patches from infected human erythrocytes without compromising seal quality.

3.7. Differing effects of pronase E on the two faces of the channel

Because our findings suggest that cytosolic components affect PSAC inactivation, we next examined the effects of proteases. Beginning with the pioneering work of Armstrong and colleagues [26], protease treatment has been a useful tool for probing the mechanisms of ion channel inactivation and has provided key structural insights.

Most proteases are membrane-impermeant, permitting selective application to one side of the channel at a time. Addition of pronase E to the patch pipette abrogated inactivation to nearly undetectable levels without significantly changing the initial currents in response to negative V_m (Fig. 7A, $n=6$ cells). Because loss of inactivation was never observed without application of proteases ($n=94$ cells), this finding strongly suggests digestion of one or more channel domains at the intracellular face.

Our impression was that pronase E also appeared to shorten the delay between the initiation of whole-cell recordings and the

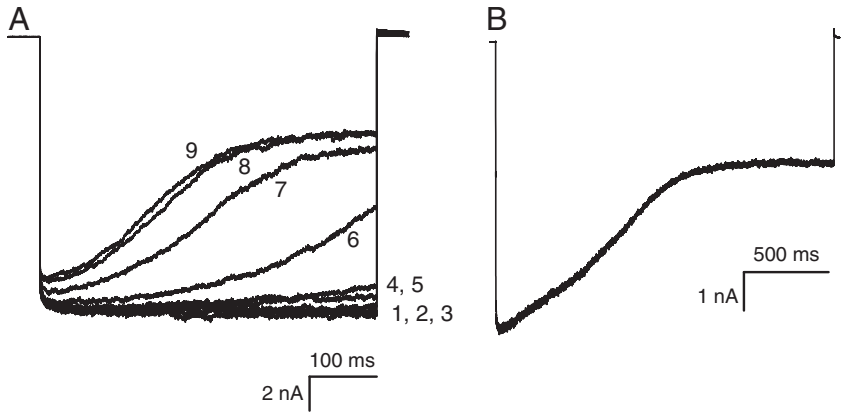

Fig. 5. Delayed onset of inactivation after achieving the whole-cell configuration. (A) Ensemble of 9 consecutive whole-cell current traces in response to V_m of −100 mV, applied as 500 ms pulses at 15 s intervals with numbers indicating their sequential order. This protocol was initiated 3 min after obtaining the whole-cell configuration. Recordings taken after those shown here yielded magnitude and kinetics similar to trace 9. (B) Inactivating response to a single pulse to V_m of −100 mV applied at 12 min after patch rupture; representative of $n=13$ cells.

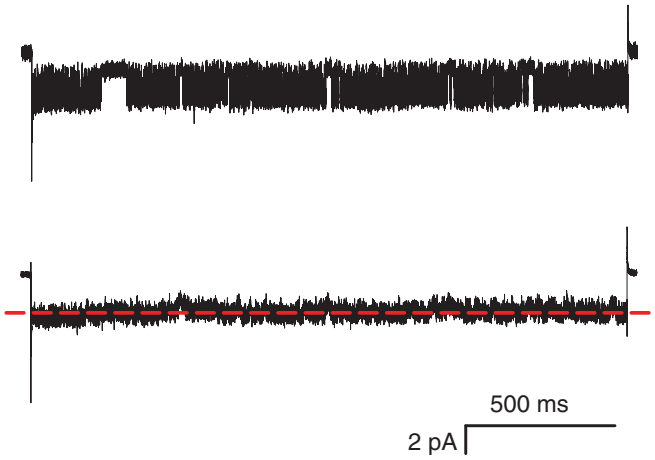

Fig. 6. Inactivation is not present in the cell-attached configuration. Upper trace shows a single channel recording during a 2 s pulse to V_m of −100 mV from a holding potential of 0 mV. Lower trace reflects the average of 7 consecutive traces collected from this channel. Bath and pipette compartments contained solution A. The dashed red line marks the mean single channel current for the entire pulse duration. Notice that the averaged response does not decrease over the course of the voltage pulse, excluding inactivation.

development of inactivation. This acceleration was somewhat variable, presumably because it depends on diffusion of protease into the intracellular compartment; for this reason, we were unable to quantify this effect. If correct, the first effect of pronase E may be to speed washout of the cytosol through proteolysis of RBC cytoskeleton and other soluble intracellular proteins. With continued presence, it appears to hydrolyze key intracellular domains on the channel protein and abolish inactivation.

Addition of extracellular pronase E had no effect on the magnitude or kinetics of inactivation, but did cause some run-down of PSAC activity (Fig. 7B, $n = 5$ cells). Inactivation was also unaffected in experiments using cells treated with pronase E in suspension and washed prior to gigaseal formation (not shown). The differing effects of this protease applied to the two sides of the membrane provide additional evidence for an important role of rearrangements at the channel's cytoplasmic face in PSAC inactivation.

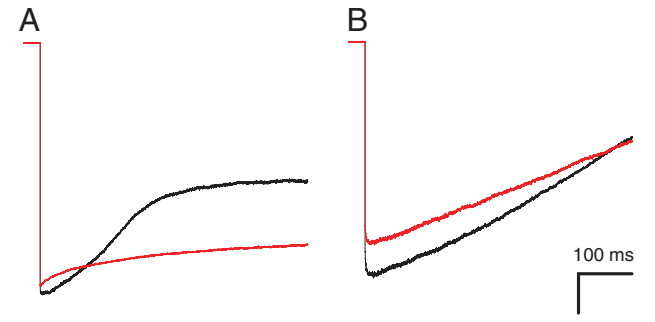

Fig. 7. Intracellular, but not extracellular, protease abolishes inactivation. (A) Whole-cell currents with 100 μg/mL pronase E in the pipette compartment. The black trace was recorded immediately after full development of inactivation; the red trace was recorded several minutes later and demonstrates loss of inactivation. (B) Whole-cell currents on a separate cell before (black trace) and approximately 40 min after addition of 100 μg/mL pronase E to the bath compartment (red trace). Traces recorded between the two shown exhibited similar levels of inactivation. Recordings in both panels used solution A in bath and pipette compartments. Vertical scale bar represents 2.3 nA (panel A) and 1.0 nA (B).

3.8. Acidic N- and C-terminal sequences of CLAG3

The recent identification of parasite *clag3* genes as determinants of PSAC provides a molecular handle for examining the structural basis of inactivation [8]. Because our studies suggest movement of a cytoplasmic domain through the membrane's electric field, we examined charge density on the CLAG3 protein and identified negatively charged regions at both ends of the protein (Fig. 8A). The C-terminus of the protein is particularly enriched for acidic residues, with Asp^- and Glu^- accounting for 26 of the last 100 residues. Moreover, biochemical studies of CLAG3 after addition of an epitope FLAG tag to the C-terminus indicate that this end of the protein is intracellular, also consistent with a role in inactivation [8]. Movement of this charged region when negative membrane potentials are applied can conservatively account for the observed voltage-dependent inactivation reported here (Fig. 8B). However, it is possible that the inactivating particle reported here is formed either by another domain within CLAG3 or by a charged component of an unrelated protein. Such a protein may be an unidentified PSAC subunit or a protein that transiently interacts with the channel.

4. Discussion

Here, we identify and characterize voltage-dependent inactivation in the plasmodial surface anion channel. While voltage-dependent inactivation has been extensively characterized in Na^+, K^+, and Ca^+ channels, it has been reported in only a few anion channels [33].

The key features of PSAC inactivation are detection only in the whole-cell configuration, delayed onset after achieving this configuration, voltage dependence for both inactivation and recovery with a relatively small z_g, and sensitivity to intracellular but not extracellular protease treatment. Although other mechanisms remain possible, we propose the simplified structural model shown in Fig. 8B. In this model, a cytoplasmic domain of the channel is tethered to one or more soluble substances, possibly components of the underlying cytoskeleton. This association prevents pore rearrangements needed for inactivation, accounting for the absence of inactivation in cell-attached single-channel recordings and in whole-cell recordings acquired immediately after rupture of the membrane patch. After washout of the putative soluble substance in the whole-cell configuration, the cytoplasmic domain of the channel is released, derepressing inactivation. The model also accounts for the effects of intracellular pronase E. This protease appears to first accelerate development of inactivation by speeding removal of the cytoskeleton; it then abolishes inactivation by digesting the channel domain(s) whose voltage-dependent movements produce inactivation. Although acidic regions on the CLAG3 protein may be the responsible channel domain(s), there could also be unidentified subunits of PSAC that provide the required voltage-dependent charge movement.

While PSAC inactivation resembles fast inactivation in Na^+ channels [34] in that both involve rearrangements of channel domains at the cytoplasmic face and both are susceptible to intracellular protease treatment, there are some important differences. First, PSAC inactivation is seen only in the whole-cell configuration and is not present under more physiological conditions. In contrast, Na^+ channel inactivation is independent of recording configuration; indeed, it plays an essential role in excitable cells by allowing rapid termination of action potentials. Second, the rate of inactivation is significantly slower in PSAC ($t_{½} > 100$ ms at all voltages) when compared to a few milliseconds for the Na^+ channel. This difference may be important because it suggests that the cytoplasmic components on PSAC are not as freely mobile as a true “ball-and-chain”. The kinetics of inactivation may be influenced by the structural rigidity of the inactivating particle, the length of polypeptide linkers, and electrostatic and/or hydrophobic interactions between the inactivating particle and other domains. Third, PSAC's inactivation is voltage-dependent, albeit with a

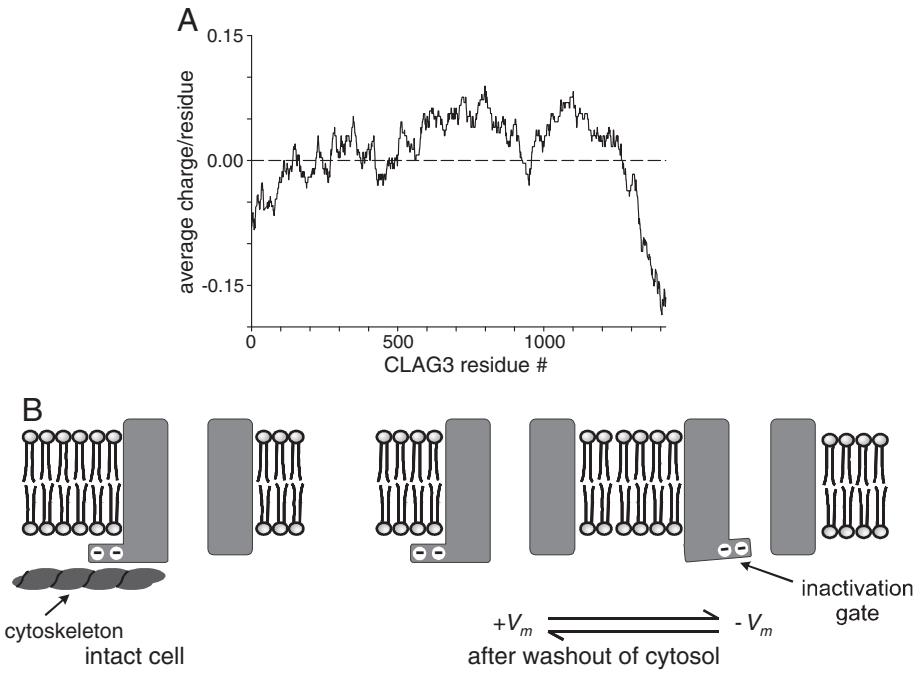

Fig. 8. (A) Charge density along the CLAG3 protein's primary sequence. The N- and C-termini of the protein correspond to residues 1 and 1417 in this plot. (B) Model for voltage-dependent inactivation. Under physiological conditions ("intact cell"), the channel is tethered to underlying cytoskeletal components and does not exhibit inactivation. Whole-cell patch-clamp washes out the cytosol and permits voltage-dependent rearrangements that reduce ionic currents. Intracellular pronase E treatment may hydrolyze this domain and abolish inactivation. The negatively charged cytoplasmic channel domain whose movement produces inactivation may correspond to the N- or C-terminus of CLAG3. Positive charges that move inward through the electric field to produce inactivation are also compatible with our findings.

relatively modest z_g. In contrast, Na^+ channel inactivation is not voltage-dependent, although this was not easily recognized because of a tight sequential link to one or more strongly voltage-dependent activation steps [35,36].

What role might PSAC inactivation play in parasite biology? A direct role appears unlikely because the required large negative V_m values are not encountered by infected erythrocytes. Nevertheless, conservation of inactivation in divergent parasite lines suggests a conserved channel domain, possibly within the N- or C-terminus of the CLAG3 protein (Fig. 8A). This domain may be conserved because of a critical role in tethering the channel protein to underlying cytoskeletal components. Directed mutagenesis of the parasite *clag3* genes combined with transport measurements may address both the structural basis and biological significance of PSAC inactivation.

Acknowledgements

We thank Ajay D. Pillai for comments on the manuscript. This research was supported by the Intramural Research Program of the National Institutes of Health, National Institute of Allergy and Infectious Diseases.

References

[1] K. Kirk, H.A. Horner, B.C. Elford, J.C. Ellory, C.I. Newbold, Transport of diverse substrates into malaria-infected erythrocytes via a pathway showing functional characteristics of a chloride channel, J. Biol. Chem. 269 (1994) 3339–3347.
[2] H. Ginsburg, S. Kutner, M. Krugliak, Z.I. Cabantchik, Characterization of permeation pathways appearing in the host membrane of *Plasmodium falciparum* infected red blood cells, Mol. Biochem. Parasitol. 14 (1985) 313–322.
[3] J.M. Upston, A.M. Gero, Parasite-induced permeation of nucleosides in *Plasmodium falciparum* malaria, Biochim. Biophys. Acta 1236 (1995) 249–258.
[4] Z.I. Cabantchik, Properties of permeation pathways induced in the human red cell membrane by malaria parasites, Blood Cells 16 (1990) 421–432.
[5] H.M. Staines, C. Rae, K. Kirk, Increased permeability of the malaria-infected erythrocyte to organic cations, Biochim. Biophys. Acta 1463 (2000) 88–98.
[6] K.J. Saliba, H.A. Horner, K. Kirk, Transport and metabolism of the essential vitamin pantothenic acid in human erythrocytes infected with the malaria parasite *Plasmodium falciparum*, J. Biol. Chem. 273 (1998) 10190–10195.
[7] S.A. Desai, S.M. Bezrukov, J. Zimmerberg, A voltage-dependent channel involved in nutrient uptake by red blood cells infected with the malaria parasite, Nature 406 (2000) 1001–1005.
[8] W. Nguitragool, A.A. Bokhari, A.D. Pillai, K. Rayavara, P. Sharma, B. Turpin, L. Aravind, S.A. Desai, Malaria parasite *clag3* genes determine channel-mediated nutrient uptake by infected red blood cells, Cell 145 (2011) 665–677.
[9] V.M. Crowley, N. Rovira-Graells, L.R. de Pouplana, A. Cortes, Heterochromatin formation in bistable chromatin domains controls the epigenetic repression of clonally variant *Plasmodium falciparum* genes linked to erythrocyte invasion, Mol. Microbiol. 80 (2011) 391–406.
[10] S. Goel, M. Valiyaveettil, R.N. Achur, A. Goyal, D. Mattei, A. Salanti, K.R. Trenholme, D.L. Gardiner, D.C. Gowda, Dual stage synthesis and crucial role of cytoadherence-linked asexual gene 9 in the surface expression of malaria parasite var proteins, Proc. Natl. Acad. Sci. U. S. A. 107 (2010) 16643–16648.
[11] G. Lisk, S.A. Desai, The plasmodial surface anion channel is functionally conserved in divergent malaria parasites, Eukaryot. Cell 4 (2005) 2153–2159.
[12] H. Iriko, O. Kaneko, H. Otsuki, T. Tsuboi, X.Z. Su, K. Tanabe, M. Torii, Diversity and evolution of the rhoph1/clag multigene family of *Plasmodium falciparum*, Mol. Biochem. Parasitol. 158 (2008) 11–21.
[13] A.D. Pillai, M. Pain, T. Solomon, A.A. Bokhari, S.A. Desai, A cell-based high-throughput screen validates the plasmodial surface anion channel as an antimalarial target, Mol. Pharmacol. 77 (2010) 724–733.
[14] J.V. Cohn, A. Alkhalil, M.A. Wagner, T. Rajapandi, S.A. Desai, Extracellular lysines on the plasmodial surface anion channel involved in Na^+ exclusion, Mol. Biochem. Parasitol. 132 (2003) 27–34.
[15] G. Lisk, S. Scott, T. Solomon, A.D. Pillai, S.A. Desai, Solute-inhibitor interactions in the plasmodial surface anion channel reveal complexities in the transport process, Mol. Pharmacol. 71 (2007) 1241–1250.
[16] S.A. Desai, Open and closed states of the plasmodial surface anion channel, Nanomedicine 1 (2005) 58–66.
[17] H.M. Staines, T. Powell, J.C. Ellory, S. Egee, F. Lapaix, G. Decherf, S.L. Thomas, C. Duranton, F. Lang, S.M. Huber, Modulation of whole-cell currents in *Plasmodium falciparum*-infected human red blood cells by holding potential and serum, J. Physiol. 552 (2003) 177–183.
[18] A. Alkhalil, J.V. Cohn, M.A. Wagner, J.S. Cabrera, T. Rajapandi, S.A. Desai, *Plasmodium falciparum* likely encodes the principal anion channel on infected human erythrocytes, Blood 104 (2004) 4279–4286.
[19] G. Lisk, S.A. Desai, Improved perfusion conditions for patch-clamp recordings on human erythrocytes, Biochem. Biophys. Res. Commun. 347 (2006) 158–165.
[20] S. Baumeister, M. Winterberg, C. Duranton, S.M. Huber, F. Lang, K. Kirk, K. Lingelbach, Evidence for the involvement of *Plasmodium falciparum* proteins in the formation of new permeability pathways in the erythrocyte membrane, Mol. Microbiol. 60 (2006) 493–504.

[21] C.M. Armstrong, Inactivation of the potassium conductance and related phenomena caused by quaternary ammonium ion injection in squid axons, J. Gen. Physiol. 54 (1969) 553–575.
[22] P. Brehm, R. Eckert, Calcium entry leads to inactivation of calcium channel in Paramecium, Science 202 (1978) 1203–1206.
[23] C.M. Armstrong, R.P. Swenson Jr., S.R. Taylor, Block of squid axon K channels by internally and externally applied barium ions, J. Gen. Physiol. 80 (1982) 663–682.
[24] H. Matsuda, A. Saigusa, H. Irisawa, Ohmic conductance through the inwardly rectifying K channel and blocking by internal Mg^{2+}, Nature 325 (1987) 156–159.
[25] A.N. Lopatin, E.N. Makhina, C.G. Nichols, Potassium channel block by cytoplasmic polyamines as the mechanism of intrinsic rectification, Nature 372 (1994) 366–369.
[26] C.M. Armstrong, F. Bezanilla, E. Rojas, Destruction of sodium conductance inactivation in squid axons perfused with pronase, J. Gen. Physiol. 62 (1973) 375–391.
[27] T. Hoshi, W.N. Zagotta, R.W. Aldrich, Biophysical and molecular mechanisms of Shaker potassium channel inactivation, Science 250 (1990) 533–538.
[28] E.Y. Isacoff, Y.N. Jan, L.Y. Jan, Putative receptor for the cytoplasmic inactivation gate in the Shaker K^+ channel, Nature 353 (1991) 86–90.
[29] G. Yellen, The moving parts of voltage-gated ion channels, Q. Rev. Biophys. 31 (1998) 239–295.
[30] B. Hille, Ion Channels of Excitable Membranes, Sinauer Associates, Sunderand, MA, 2001.
[31] C.R. De, K. Messlinger, R.W. Carr, Conduction velocity is regulated by sodium channel inactivation in unmyelinated axons innervating the rat cranial meninges, J. Physiol. 586 (2008) 1089–1103.
[32] O.P. Hamill, A. Marty, E. Neher, B. Sakmann, F.J. Sigworth, Improved patch-clamp techniques for high-resolution current recording from cells and cell-free membrane patches, Pflugers Arch. 391 (1981) 85–100.
[33] A. Accardi, M. Pusch, Fast and slow gating relaxations in the muscle chloride channel CLC-1, J. Gen. Physiol. 116 (2000) 433–444.
[34] C.M. Armstrong, Na channel inactivation from open and closed states, Proc. Natl. Acad. Sci. U. S. A. 103 (2006) 17991–17996.
[35] F. Bezanilla, C.M. Armstrong, Inactivation of the sodium channel. I. Sodium current experiments, J. Gen. Physiol. 70 (1977) 549–566.
[36] G. Cota, C.M. Armstrong, Sodium channel gating in clonal pituitary cells. The inactivation step is not voltage dependent, J. Gen. Physiol. 94 (1989) 213–232.